Probing quantum materials with novel scanning tunneling microscopy techniques

Bastiaans, K.M.

5

A strongly inhomogeneous superfluid in an iron-based superconductor

This chapter has been published as *Nature* **571**, 541 (2019)

Although the possibility of spatial variations in the superfluid of unconventional, strongly correlated superconductors has been suggested, it is not known whether such inhomogeneities - if they exist - are driven by disorder, strong scattering, or other factors. In this chapter we use atomic-resolution Josephson scanning tunneling microscopy to reveal a strongly inhomogeneous superfluid in the iron-based superconductor $FeTe_{0.55}Se_{0.45}$. By simultaneously measuring the topographic and electronic properties, we find that this inhomogeneity in the superfluid is not caused by structural disorder or strong inter-pocket scattering, and does not correlate with variations in the energy of the Cooper pair-breaking gap. Instead, we see a clear spatial correlation between superfluid density and the quasiparticle strength, defined as the height of the coherence peak, on a local scale. This places iron-based superconductors on equal footing with the cuprates, where a similar relation has been observed on the macroscopic scale. Our results establish the existence of strongly inhomogeneous superfluids in an unconventional supercondtuctor, exclude chemical disorder and inter-band scattering as causes of the inhomogeneity, and shine light into the relation between quasiparticle character and superfluid density. When repeated at different temperatures, our technique could further help to elucidate what local and global mechanisms limit the critical temperature in unconventional superconductors.

5.1. INTRODUCTION

Superconductivity emerges when electrons pair up to form so-called Cooper pairs and then establish phase coherence to condense into the macroscopic quantum state that is the superfluid. Cooper pairing is governed by the binding energy of the pairs, Δ_{CP}, while the phase coherence (or stiffness) governs the superfluid density, n_{sf} [1]. For conventional superconductors like aluminum or lead, the superfluid density is spatially homogeneous because the lattice constant is much smaller than the Cooper pair size (usually hundreds of nanometers) and because the large superfluid density guarantees a high phase stiffness. In unconventional, strongly correlated superconductors the situation is very different for the following reasons: (i) the Cooper pair size, roughly given by the coherence length, is generally smaller than the pair size in conventional superconductors; (ii) the superfluid density is smaller (iii), more disorder exists due to dopant atoms or intrinsic tendencies for phase separation or charge order; and (iv) the sign of the superconducting gap changes. Despite much progress [2, 3], we lack a theoretical understanding of these strongly correlated superconductors. It has long been proposed that there can, in principle, exist spatial variations of the superfluid density [4, 5]. Very similar ideas have been discussed thoroughly in the context of superconductor-insulator transitions [6–8], or Bose-Einstein condensation of electronic liquids [9]. However, little is known about the local physics in such systems because of the technical challenges associated with visualizing the superfluid density on the atomic scale, especially when simultaneously probing the density of states to investigate the origin of the inhomogeneity. In this chapter we use atomic-resolution Josephson scanning tunneling microscopy to reveal a strongly inhomogeneous superfluid in the iron-based superconductor $FeTe_{0.55}Se_{0.45}$.

5.2. SPECTROSCOPY IN A JOSEPHSON STM

As we discussed in chapter 4, both the pair-breaking gap (the energy required to break Cooper pairs) and the superfluid density should be accessible through two distinct spectroscopic signatures in a tunneling contact between superconductors (Fig 5.1.a). The first one is visible in the single-particle channel, where Bogoliubov quasiparticles with energies larger than the pair-breaking gaps transport the charge, as shown in Fig 5.1.b. In the case of the Josephson scanning tunneling microscopy (STM) configuration, one of the superconductors is the tip with gap $\Delta_{CP,t}$ and the other is the sample with gap $\Delta_{CP,s}$; leading to a total gap of energy $2(\Delta_{CP,s} + \Delta_{CP,t})$ (Fig 5.1.c). The second spectroscopic feature is at bias energies close to the Fermi energy, where one can access the Cooper-pair channel which yields information about the superfluid density. Voltage-biased Josephson tunneling in our STM configuration differs somewhat from the case of planar junctions: the capacitive energy E_C is

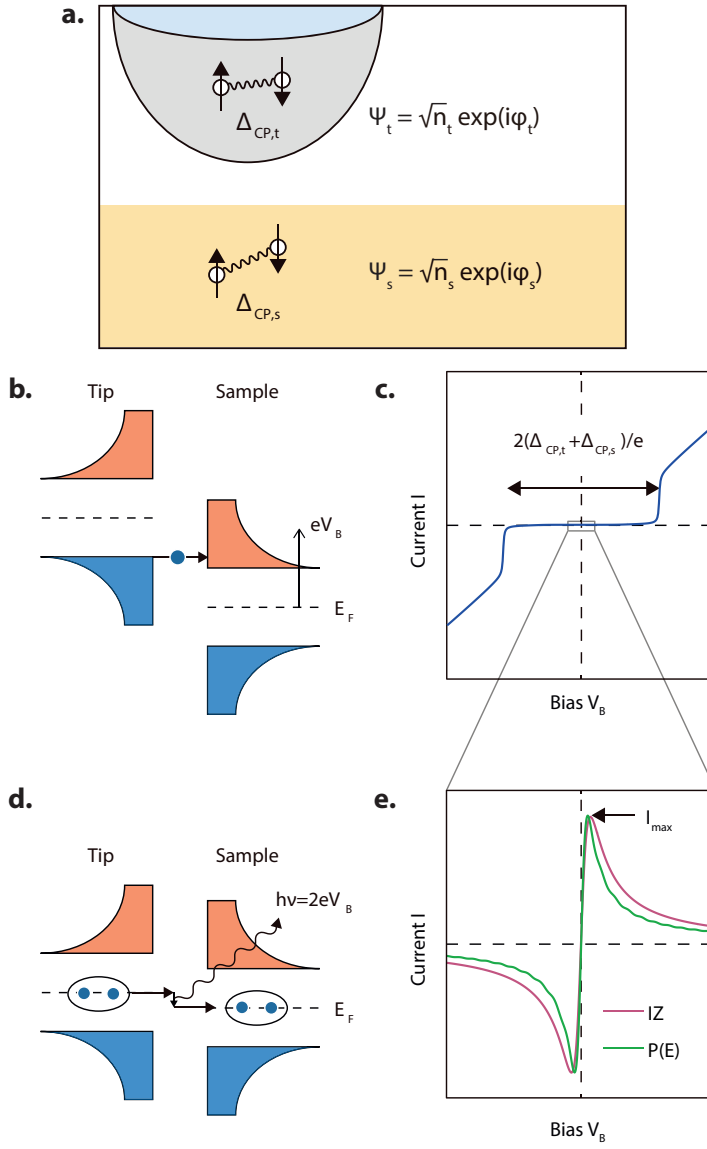

Figure 5.1: **Principles of Josephson Scanning Tunneling Microscopy. a.** Schematic of the Josephson junction consisting of tip (t) and sample (s). **b.** Schematic energy diagram of quasiparticle tunneling between tip and sample. Black lines indicate the density of states (horizontal axis) as a function of energy (vertical axis); filles / empty states are denoted with blue / red; dashed lines indicate the Fermi level E_F. When the voltage bias V_B is larger than $(\Delta_{CP,s} + \Delta_{CP,t})/e$, quasiparticles can tunnel. **c.** Current-Voltage I-V characteristic curve for quasiparticle tunneling. **d.** Schematic of inelastic Cooper-pair tunneling in a Josephson junction. Cooper pairs interacts with the environment by emitting energy (wavy arrow) and subsequently tunnels across the junction. **e.** Simulates I-V curves for Cooper-pair tunneling. Both curves exhibit a maximum I_{max} at finite bias which is proportional to I_C^2.

much bigger than the Josephson energy, E_J, turning the environmental impedance into a relevant quantity, and, in our case, the thermal energy is relatively high.

We calculate the current-voltage characteristics of Josephson tunneling based on two different theoretical frameworks: IZ and P(E). The former, named after its developers Ivanchenko and Zil'berman, models the environment as Ohmic and assumes that the thermal energy exceeds the Josephson energy [10]. The latter, named after the probability function central to the theory, is a quantum mechanical treatment of Cooper pair tunneling in ultra-small junctions [11]. For our specific configuration, the qualitative predictions from both theoretical descriptions are similar: a Josephson current flows at small bias, with a maximum within a few microvolts around the Fermi energy (Fig 5.1.d-e), reflected in a conductance spectrum that shows a peak at zero applied bias. The maximum Josephson current (arrow in Fig 5.1.e) is proportional to the square of the critical current I_C of the junction.

In in single band, s-wave superconductors the superfluid density is then proportional to $(I_C R_N)^2$, where R_N is the normal state resistance, and the interpretation is straightforward: it is the density of condensed Cooper pairs [12]. In multi-band or unconventional superconductors, the superfluid density defined this way represents the superposition of different contributions from different bands, with weights depending on the relative phase,

$$I_C R_N \propto \sum_i \sqrt{n_i} \cos \chi_i, \tag{5.1}$$

where n_i are the individual superfluid densities of the different bands and χ_i their relative phases (see also appendix 5.A and 5.B). When tunneling locally, one has to convert from a band basis to an orbital basis and consider the overlap of each kind of the orbitals with different bands, as well as the individual tunneling matrix elements for the different orbitals. One can still extract spatial variations in the superfluid using the definition above, if the ratios between the tunneling matrix elements are spatially constant or when the superconducting phase is not strongly related to the orbitals. But importantly, the superfluid density thus defined cannot be simply interpreted as the total density of Cooper pairs for unconventional or multi-band superconductors, including the one investigated here. Notably, the multiplication with R_N in the $(I_C R_N)^2$ product also allows to disentangle the measured superfluid density from variations in the coupling between the tip and the superfluid which might vary spatially [13, 14]. Spatially imaging a superfluid using Josephson STM techniques [15] has thus far been achieved in two instances. First, a pair density wave was discoverd in a copper oxide sample [13], by exfoliating pieces of the sample onto the STM tip and imaging it with a resolution of about 1 nm. Second, the superfluid of a Pb(111) surface was resolved with atomic resolution, by using the sample material to coat the STM tip [14].

In this chapter, we investigate the unconventional iron-based superconductor $FeTe_{0.55}Se_{0.45}$. Iron-based superconductors are moderately to strongly correlated, with Hund's rule and orbital selectivity playing important roles [16]. We chose $FeTe_{0.55}Se_{0.45}$ because it encompasses the key properties of unconventional superconductivity. Furthermore, its nodeless gap structure [17, 18] and the possibility to scan at low junction resistances facilitate the Josephson experiments described below. $FeTe_{0.55}Se_{0.45}$ is considered not to be in the dirty BCS limit and has a low average superfluid density similar to cuprate high temperature superconductors [19, 20]. We cleave the single crystals at 30 K and insert the samples into our cryogenic STM system with rigorous electronic filtering (as described in chapters 2 and 4). All measurements were performed at an effective electron temperature of 2.2 K. The topograph (Fig. 5.2.a) shows atomic resolution and contrast differences that stem from the tellurium or selenium inhomogeneities; we further verify that the interstitial iron concentration is negligible. Similar to chapter 4, we use a mechanically sharpened platinum iridium wire with its apex coated with lead, which is a s-wave superconductor with a relatively large gap of ~ 1.3 meV [14].

These preparations enable us to acquire Josephson tunneling spectra and maps on $FeTe_{0.55}Se_{0.45}$. Figure 5.2 shows current and differential conductance spectra acquired at the location marked by a cross in Fig. 5.2.a. The data agrees well with expectations from the IZ and P(E) models, and reproduces small oscillation features seen previously on elemental superconductors and explained by a tip-induced antenna mode in chapter 4 and in references [14, 21]. Decreasing the junction resistance shows the increase of the critical current expected for a Josephson tunneling junction (as shown in Fig. 5.2). The rate of the increase is lower than expected for simple s-wave junctions but more consistent with theoretical predictions for a $S\pm$ pairing symmetry in the sample, where states with both positive and negative gap tunnel [22]. We further note a small kink in the Josephson current at $25\mu eV$ of yet unknown origin.

5.3. VISUALIZING THE INHOMOGENEOUS SUPERFLUID

In Figs 5.3.a and 5.3.b, we show an atomic-resolution map of the superfluid density as defined in section 5.2, extracted from ~ 16,000 individual spectra, and the topographic image, registered spatially to each other on the atomic scale. The most striking finding of our experiment is the strong inhomogeneity of the superfluid over length scales of the order of the coherence length, a few nanometers. We show in Fig. 5.3.c a series of individual raw spectra normalized by the normal state resistance to illustrate these changes. The inhomogeneities are not periodic; a possible underlying pair density wave is below our sensitivity. Our setup allows us to measure topographic and electronic properties in the same field of view and thus inves-

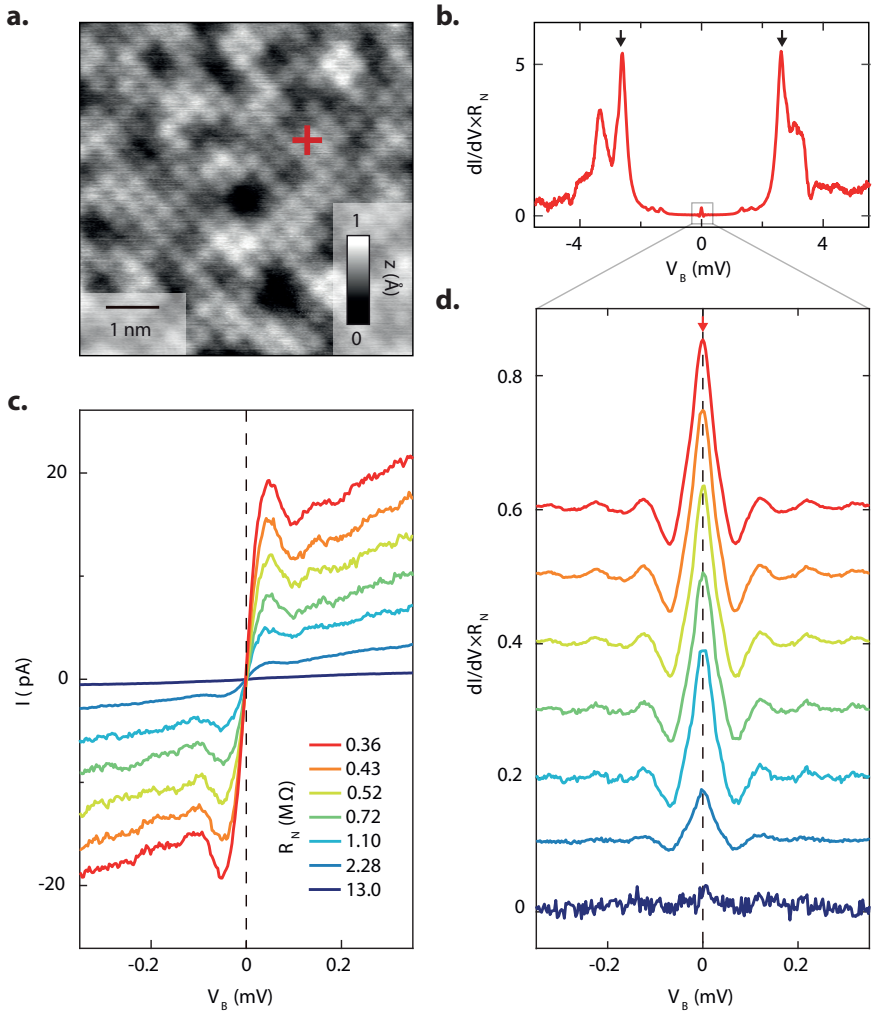

Figure 5.2: **Josephson tunneling spectra on** $FeTe_{0.55}Se_{0.45}$**. a.** Atomically resolved topographic image (setup conditions $V_{set} = -10$mV, $I_{set} = 5$nA). Brighter (darker) atoms correspond to Te (Se). **b.** Differential conductance spectrum acquired at the location of the red cross in (a), multiplied by the normal state resistance. Black arrows indicate the coherence peaks. The Josephson current can be observed at small bias. Setup conditions: $V_{set} = -10$ mV, $I_{set} = 30$nA, $V_{mod} = 20\mu V_{pp}$ **c.** Current-voltage characteristic for different normal state resistances. All spectra are acquired with $V_{set} = -10$ mV. **d.** Differential conductance spectra acquired with the same set-up conditions as in c and a lock-in modulation $V_{mod} = 20\mu V_{pp}$, multiplied by the respective normal state resistance, yielding a dimensionless quantity.

tigate possible causes for the inhomogeneous superfluid. The most obvious possible causes might be structural disorder and strong quasiparticle scattering. The structural disorder stems from the effective FeSe and FeTe alloying that is clearly visible in the topographic images (Fig. 5.2.a and Fig. 5.3.a). Surprisingly, the variations in the superfluid are not correlated to these structural features, with the exception of a few impurity atoms that lead to a strong suppression of the Josephson current. The strength of the quasiparticle scattering is visible in quasiparticle interference (QPI) pattern and is dominated by inter-pocket scattering in $FeTe_{0.55}Se_{0.45}$ [17]. We identify areas of strong scattering with red contours in Fig. 5.3.d, which are obtained by Fourier-filtering the QPI data in order to distinguish between strong and weak scattering regions. Again, there is no correlation between these regions and the superfluid density. We cannot exclude that the superfluid density is influenced by potential scatterers not visible in our measurement, remnant short range magnetic order, or possible phase separations at higher energies. Given the putative $s\pm$ pairing symmetry of the sample as mentioned above, one could also consider a scenario involving spatially varying tunneling matrix elements between the tip and orbitals coupled to opposite-sign gaps, leading to a spatially varying suppression of the Josephson current [22]. However, in $FeTe_{0.55}Se_{0.45}$, the gap sign is not strongly related to the orbital character [18, 23], and we do not observe the imprint that a relative change in the tunneling matrix elements of the different orbitals would leave on the local density of states and the topography. More generally, the fact that such prominent effects as the chemical disorder and the inter-pocket QPI do not influence the superfluid indicates that the inhomogeneity in the superfluid density is intrinsic.

We now return to the relation between the pair-breaking gap and the superfluid density. We extract the pair-breaking gap energy, as well as the height of the coherence peaks, which will prove to be important later, by fitting the coherence peaks of each spectrum to find the energy of the maxima. Figure 5.3.e shows the gap map for the same field of view as the Josephson map; the gap variations agree with previous reports [24]. It is clear that the pair-breaking gap is independent of the superfluid density. Instead we find a correlation to the quasiparticle character, as described in the following section.

5.4. CORRELATION BETWEEN SUPERFLUID DENSITY AND QUASIPARTICLE COHERENCE

In unconventional superconductors, there is a recurring theme that connects quasiparticle excitation line-shapes with the presence of superconductivity: Photoemission demonstrated that the incoherent quasiparticles in the normal state become coherent below the critical temperature [18, 25]. Previous STM measurements showed Bogoliubov QPI patterns at low energies which are even sharper than theory would

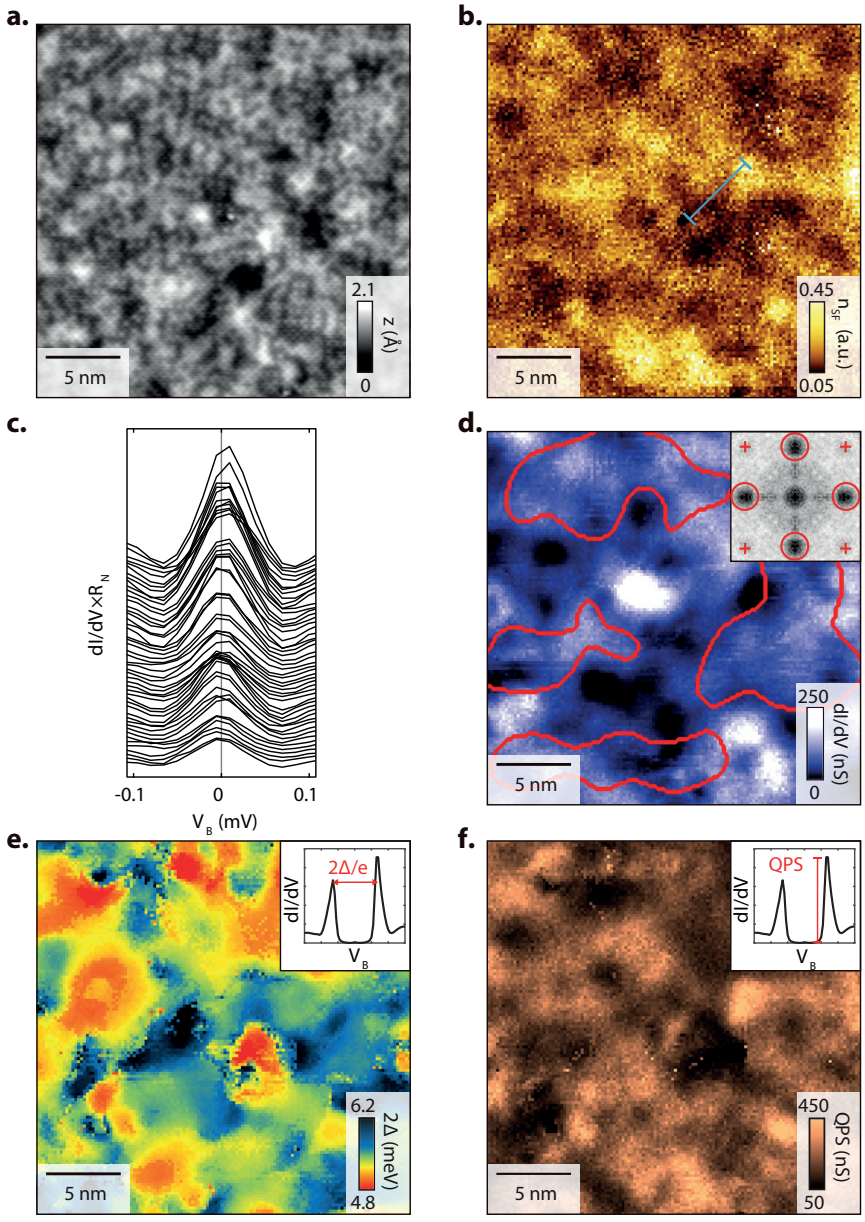

Figure 5.3: **Visualizing the superfluid in** $FeTe_{0.55}Se_{0.45}$**. a.** $25 \times 25\ nm^2$ topographic image of $FeTe_{0.55}Se_{0.45}$ ($V_{set} = -6$ mV, $I_{set} = 0.12$ nA). **b.** Spatially resolved map of $(I_C R_N)^2$ representing the superfluid density as discussed in section 5.2 ($V_{set} = -6$ mV, $I_{set} = 5$ nA, $V_{mod} = 30\,\mu V_{pp}$). **c.** Series of differential conductance spectra multiplied by the normal state resistance around E_F along the blue line in (b). **d.** Conductance map at VB =+3.6 mV. Areas with strong quasiparticle interference patterns are marked by red contours, which are obtained by Fourier-filtering the QPI data using the filter shown in the inset (red circle). Inset: Fourier transform, with crosses at the Bragg peak locations. **e.** Pair-breaking gap map, $\Delta = \Delta_{CP,s} + \Delta_{CP,t}$. **f.** Coherence peak-height map (QPS), extracted simultaneously with the pair-breaking gap. All maps in (b-f) were obtained in the same field of view as the topography in (a), registered to each other using the simultaneously acquired topographs. Setup conditions for (d-f): $V_{set} = -6$ mV, $I_{set} = 0.3$ nA, $V_{mod} = 400\,\mu V_{pp}$.

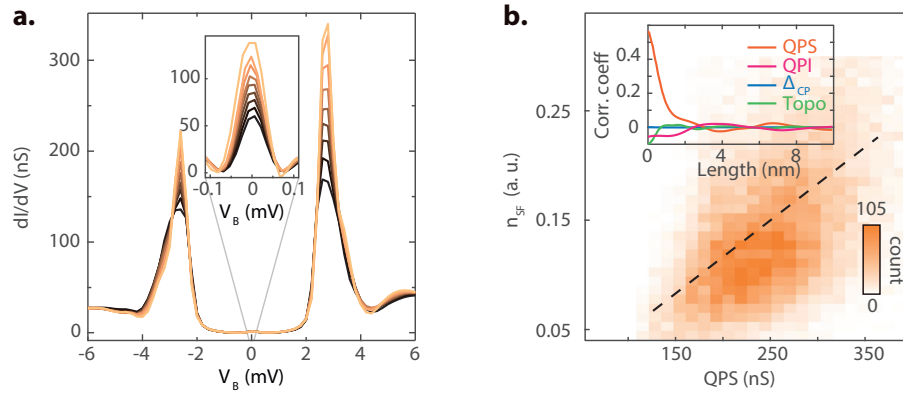

Figure 5.4: **Correlation between $(I_C R_N)^2$ and coherence peak-height. a.** Sorted spectra of the coherence peak-height (V_{set} = −6mV, I_{set} = 0.3 nA) and the zero-bias Josephson peak (V_{set} = −6 mV, I_{set} = 5 nA). Spectra were sorted by binning of the superfluid density map shown in Fig. 5.3.b. The colors correspond to the quasiparticle strength in Fig. 5.3.f. **b.** Correlation between coherence peak-height and superfluid density extracted from the $(I_C R_N)^2$ product as discussed in section 5.2, yielding a correlation factor of 0.58 (dashed line). The inset shows the distance dependence of the correlation factors between the superfluid density and QPS, QPI, Δ_{CP} and topographic height.

predict, but vanish well below the gap energy [26]. Those measurements suggest a remarkable relation between the average quasiparticle excitation spectrum and superconductivity, but do not address the inhomogeneous character of unconventional superconductors. Although recently a relation between superfluid density and quasiparticle character has been conjectured to hold also locally for single-layer cuprates [27], direct experimental evidence is so far missing. Our measurement allows us to extract the quasiparticle strength (QPS), which we define phenomenologically as the height of the coherence peak (Fig. 5.3.f), and relate it directly to the superfluid density at the same location. Indeed, we find a striking correlation between the superfluid density and the QPS over the whole field of view, with a linear correlation coefficient of 0.58 (Fig. 5.4). Although this phenomenology cannot be explained by an existing theory, it points towards a local mechanism behind the relation found by photoemission experiments - a condition fulfilled by pinned thermal phase fluctuations and glassy superconductivity [1, 28].

The length scales of the superfluid inhomogeneity and of its correlation to the QPS (Fig.5.4.b, inset) are of the same order as the average electron-electron distance. Therefore, our measurement indicates that the Cooper pairs in $FeTe_{0.55}Se_{0.45}$ are very local: they are small in size and have little overlap in comparison to the ones in conventional superconductors. We can further compare this situation to the crossover from momentum-condensed pairs described by BCS and completely local pairs described by Bose-Einstein condensation (BEC) which has been demonstrated

with ultracold atomic gases for s-wave superfluids [29, 30]. There also exist indications for pairing in the BEC or crossover regime close to superconductor-insulator transitions and in the cuprates; in $FeTe_{0.55}Se_{0.45}$ the phenomenology is not conclusive [18, 31]. Our data points towards local pairs in $FeTe_{0.55}Se_{0.45}$, but we note that in a multi-band, putative sign-changing superconductor, we expect the situation to be more complicated than the realization seen in ultracold atomic gases, and both better theory and more experiments are needed.

5.5. CONCLUSIONS AND OUTLOOK

In this chapter we have detected and directly imaged a strongly inhomogeneous superfluid and simultaneously measured the electronic and topographic properties in the same field of view, with atomic resolution. We found that the superfluid inhomogeneity is not caused by the structural disorder resulting from the Se/Te alloying, by the inter-pocket scattering, or by the variations of the pair-breaking gap energy (Fig. 5.4b, inset). Instead, the superfluid density shows strong positive correlation with the sharpness of the quasiparticle peak: Superconductivity appears to be needed for coherent quasiparticles, locally on the length scale of cooper pairing. It will be instructive to use the techniques described here to investigate the superfluid density in other materials, including superconductor-insulator transitions, disordered conventional superconductors, or twisted bilayer graphene [32, 33]. Lastly, we anticipate that future temperature-dependent superfluid density and gap measurements will elucidate what local and global mechanisms limit T_C in unconventional superconductors.

APPENDICES

5.A. ACCESSING THE SUPERFLUID DENSITY WITH JOSEPHSON STM

In Josephson Scanning Tunneling Microscopy (JSTM) [34], the Josephson junction [35] is formed between a STM tip and sample (both superconducting) which are separated by a vacuum barrier. The tunneling current of Cooper pairs contains information about the superfluid in both sample and tip. Starting from the wavefunctions of the superconductors on the tip (t) and the sample (s),

$$\Psi_{s,t} = \sqrt{n_{SF,s(t)}} \exp\{-i\phi_{s(t)}\}, \tag{5.2}$$

where $n_{SF,s(t)}$ is the superfluid density and $\phi_{s(t)}$ the phase of the condensate in the sample or tip, it can be shown that the supercurrent follows the Josephson relation

$$I = I_C \sin \phi_s - \phi_t, \tag{5.3}$$

with

$$I_C = \kappa \sqrt{n_{SF,s}} \sqrt{n_{SF,t}}, \tag{5.4}$$

(κ is a coupling constant) being the maximum (critical) supercurrent that the junction can sustain. Assuming the superfluid density in the tip to be constant, one can treat the critical supercurrent as a measure to probe the superfluid density in the sample. We note that the while the relation between critical current and superfluid density is straightforward in single band s-wave superconductors [36, 37], it can become more complicated in multiband systems, where we the critical current is related to an effective superpositions of superfluid densities [38–43]. Because the ratio between tunneling elements into different orbitals is spatially constant, and because the gap sign is only weakly coupled to the different orbitals, the changes in I_C that we measure reflect changes of the superfluid density in the sample.

5.B. DETERMINING THE CRITICAL CURRENT FROM JOSEPHSON TUNNELING SPECTRA

To extract the critical supercurrent from our spectra, we fit the conductance spectra with the use of the IZ model [10]. Taking the derivative of the IZ formula with respect to the voltage we get:

$$dI/dV = \frac{I_C^2 Z_{env}}{2} \frac{V_C^2 - V^2}{(V^2 + V_C^2)^2}, \tag{5.5}$$

We fit our spectrum based on the above formula with free fitting parameters being the pre-factor $I_C^2 Z_{env}/2$ and V_C. A typical IZ fit of the conductance spectrum is shown in Fig. 5.5.

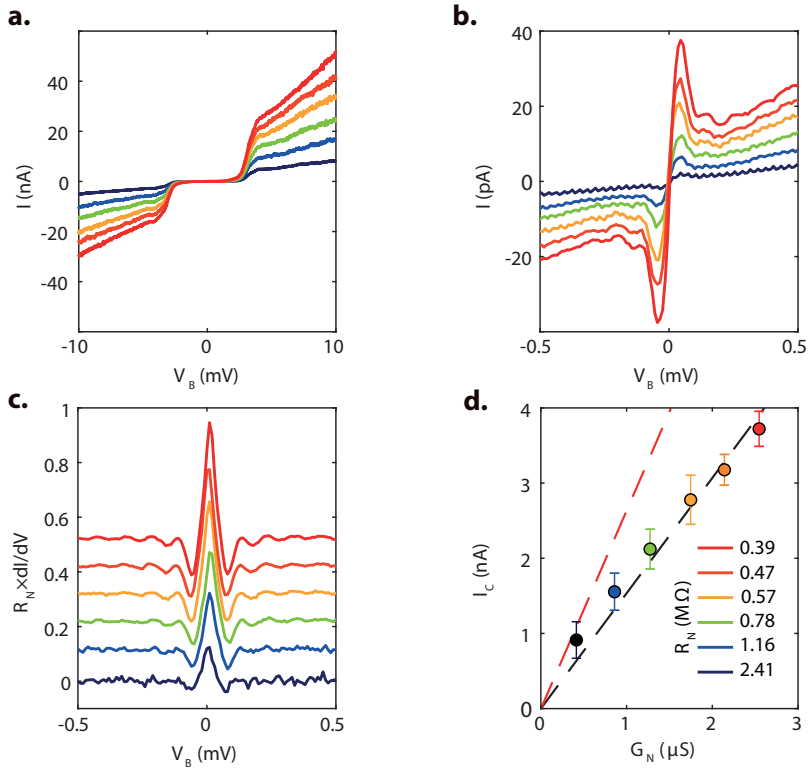

Figure 5.5: **Josephson tunneling spectroscopy in the Pb /** $FeTe_{0.55}Se_{0.45}$ **junction. a-b.** R_N-dependent I-V curves. **c.** R_N-dependent dI / dV curves multiplied by R_N corresponding to I-V curves in (a-b). Curves are offset for clarity. When decreasing R_N, Cooper-pair tunneling induced zero bias peak and small modulations with period of 0.1 meV become more pronounced. **d.** The linear relation (black dashed line) between the critical Josephson current and the normal state conductance. The red dashed line corresponds to AB-formula for a asymmetry Josephson junction where two superconductor electrodes have same s-wave symmetry with different sizes of the pair-breaking gap ($\Delta_{CP,t}$ = 1.30 meV and $\Delta_{CP,s}$ = 1.68 meV).

According to the IZ model the maximum (I_{max}) in the I-V characteristics is related to the critical supercurrent in the following way,

$$I_C = \sqrt{\frac{8 I_{max} e k_B T}{\hbar}}. \tag{5.6}$$

Hence, we can use the maximum from our I-V curves and use the above formula for quantifying I_C (we use $T = 2.2$ K which is equal to our measurement temperature). In Fig. 5.5, we plot I_C as function of normal junction conductance $G_N = (R_N)^{-1}$. A linear trend is observed which is consistent with previous theoretical works. A linear fit to our data gives a slope of 1.534 meV which is used to estimate Δ_s from the formula of an asymmetric junction [44],

$$I_C R_N = \frac{2}{e} \frac{\Delta_{CP,t}\Delta_{CP,s}}{\Delta_{CP,t} + \Delta_{CP,s}} K\left(\left|\frac{\Delta_{CP,t} - \Delta_{CP,s}}{\Delta_{CP,t} + \Delta_{CP,s}}\right|\right), \tag{5.7}$$

where $K(x)$ is the elliptic integral function of first kind. Assuming $\Delta_{CP,t} = 1.3$ meV we find $\Delta_{CP,s)} = 0.67$ meV. This is to be compared with the gap that we read from our conductance spectra. We find that the coherence peak is located at 3.08 meV. Subtracting $\Delta_{CP,t}$ gives an estimation of $\Delta_{CP,s} = 1.68$ meV. We believe that the reason for this deviation can be attributed to the unconventional superconducting nature of $FeTe_{0.55}Se_{0.45}$. Sign-changing gaps have been shown to influence the Josephson tunneling[22, 38–43]. It has been predicted theoretically that for Cooper pair tunneling between a conventional s-wave superconductor and an unconventional $s\pm$ multiband superconductor (here $FeTe_{0.55}Se_{0.45}$) I_C still grows linearly with G_N. However, for that case the slope is expected to be lower. Such reduction of Josephson current was also observed in a multiband superconductor without sign changing using a s-wave superconducting tip [43]. We expect that better calculations of the orbital-decomposed gap structure and their individual tunneling processes allow for quantitative comparisons with our data.

5.C. VISUALIZING THE SUPERFLUID DENSITY FOR SAMPLES WITH INHOMOGENEOUS NORMAL STATE JUNCTION RESISTANCE

To visualize the spatial variations of the superfluid density, we record differential conductance spectroscopic maps on a grid of points (r_x, r_y) and fit each spectrum using the IZ model described in the previous section. This allows us to construct atomic-scale $I_C(\mathbf{r})$ maps, i.e. the magnitude of the critical supercurrent as a function of location. Figure 5.6.a-b show an example of these maps on the same $25 \times 25 nm^2$ field of view, obtained using opposite setup bias Fig. 5.6.a -10 mV and Fig. 5.6.b +10 mV). These maps reveal spatial variations of the critical supercurrent on a small length scale of a few nanometers. However, we notice that these two maps are not well consistent. This is because I_C (the measured critical current of the junction) is

influenced by the single-particle tunneling transmission rate represented by $(R_N)^{-1}$ at each point (r_x, r_y). To allow for direct measurement of intrinsic variations of the superfluid density we take the product of the measured $I_C(\mathbf{r})$ with $R_N(\mathbf{r})$ (see Ref. [13]). Figures 5.6.c-d show the measured $R_N(\mathbf{r})$ images in the same field of view as the $I_C(\mathbf{r})$ maps for both bias polarities. The $R_N(\mathbf{r})$ are obtained by summing over all spatial resolved differential conductance layers $g(\mathbf{r})$ and divide by the size of the energy window. The product of measured $(I_C(\mathbf{r})\mathbf{R_N}(\mathbf{r}))^2$ enables us to deduce the spatial variations of the superfluid density.

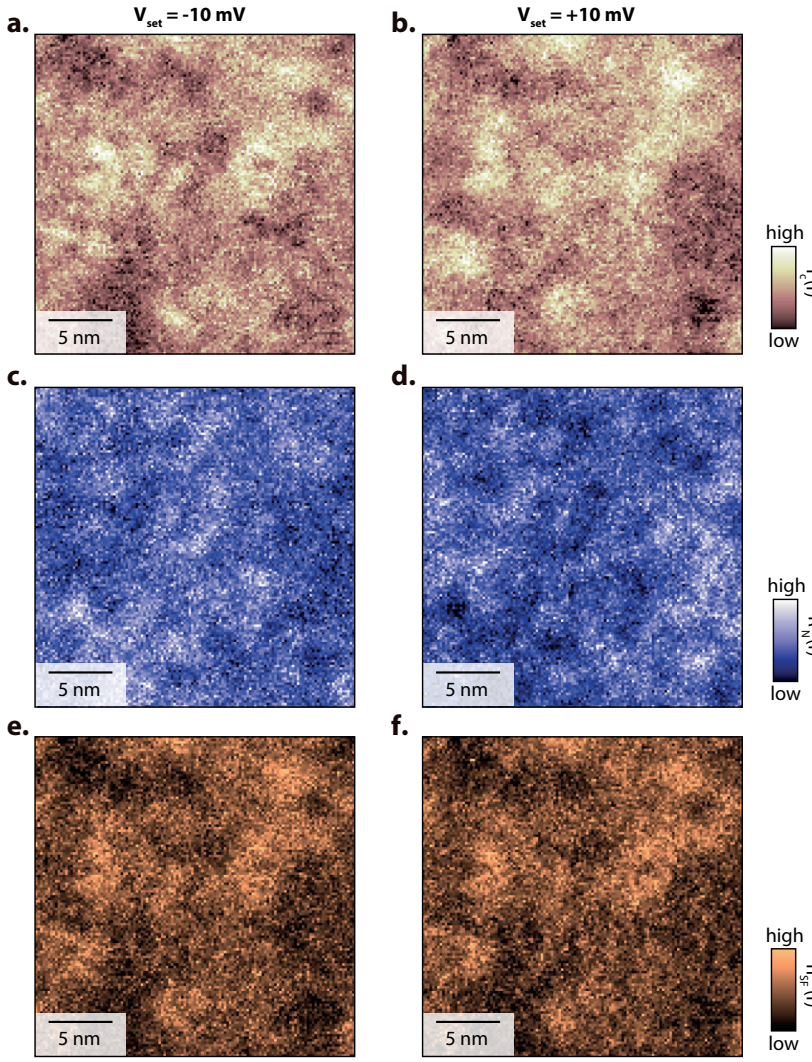

Figure 5.6: **Superfluid density maps with inhomogeneous normal state resistance. a-b.** The critical Josephson current I_C map. **c-d.** The spatial variations of the normal state resistance R_N. **e-f.** The $(I_C R_N)^2$ map associated with the superfluid density. The left (right) column were acquired with set-up bias of -10 mV (+10 mV) and set-up current of 10 nA. To map the intrinsic superfluid density, it is necessary to normalize the measured I_C by multiplying R_N. Topographs are simultaneously measured and used to align different maps.

BIBLIOGRAPHY

[1] V. J. Emery and S. A. Kivelson, *Importance of phase fluctuations in superconductors with small superfluid density,* Nature **374**, 434 (1995).

[2] F. Wang and D.-H. Lee, *The electron-pairing mechanism of iron-based superconductors,* Science **332**, 200 (2011).

[3] B. Keimer, S. A. Kivelson, M. R. Norman, S. Uchida, and J. Zaanen, *From quantum matter to high-temperature superconductivity in copper oxides.* Nature **518**, 179 (2015).

[4] P. Fulde and R. A. Ferrell, *Superconductivity in a strong spin-exchange field,* Phys. Rev. **135**, A550 (1964).

[5] A. I. Larkin and Y. N. Ovchinnikov, *Nonuniform state of superconductors,* Zh. Eksperim. i Teor. Fiz. **47** (1964).

[6] A. Ghosal, M. Randeria, and N. Trivedi, *Spatial inhomogeneities in disordered d-wave superconductors,* Phys. Rev. B **63**, 020505 (2000).

[7] M. V. Feigel'man and L. B. Ioffe, *Superfluid density of a pseudogapped superconductor near the superconductor-insulator transition,* Phys. Rev. B **92**, 100509 (2015).

[8] K. Bouadim, Y. L. Loh, M. Randeria, and N. Trivedi, *Single-and two-particle energy gaps across the disorder-driven superconductor–insulator transition,* Nature Physics **7**, 884 (2011).

[9] I. Božović, J. Wu, X. He, and A. T. Bollinger, *What is really extraordinary in cuprate superconductors?* Physica C **558**, 30 (2019).

[10] Y. M. Ivanchenko and L. A. Zil'Berman, *The Josephson Effect in Small Tunnel Contacts,* Sov. Phys. JETP **28**, 1272 (1969).

[11] G.-L. Ingold, H. Grabert, and U. Eberhardt, *Cooper-pair current through ultrasmall josephson junctions,* Phys. Rev. B **50**, 395 (1994).

[12] O. Naaman, W. Teizer, and R. C. Dynes, *Fluctuation dominated josephson tunneling with a scanning tunneling microscope,* Phys. Rev. Lett. **87**, 097004 (2001).

[13] M. H. Hamidian, S. D. Edkins, S. H. Joo, A. Kostin, H. Eisaki, S. Uchida, M. J. Lawler, E.-A. Kim, A. P. Mackenzie, K. Fujita, J. Lee, and J. C. Davis, *Detection of a cooper-pair density wave in bi 2 sr 2 cacu 2 o 8+ x,* Nature **532**, 343 (2016).

[14] M. T. Randeria, B. E. Feldman, I. K. Drozdov, and A. Yazdani, *Scanning josephson spectroscopy on the atomic scale,* Phys. Rev. B **93**, 161115 (2016).

[15] M. Graham and D. K. Morr, *Imaging the spatial form of a superconducting order parameter via josephson scanning tunneling spectroscopy,* Phys. Rev. B **96**, 184501 (2017).

[16] Z. P. Yin, K. Haule, and G. Kotliar, *Kinetic frustration and the nature of the magnetic and paramagnetic states in iron pnictides and iron chalcogenides,* Nature Materials **10**, 932 (2011).

[17] T. Hanaguri, S. Niitaka, K. Kuroki, and H. Takagi, *Unconventional s-wave superconductivity in fe (se, te),* Science **328**, 474 (2010).

[18] H. Miao, W. H. Brito, Z. P. Yin, R. D. Zhong, G. D. Gu, P. D. Johnson, M. P. M. Dean, S. Choi, G. Kotliar, W. Ku, X. C. Wang, C. Q. Jin, S.-F. Wu, T. Qian, and H. Ding, *Universal* $2\Delta_{max}/k_B T_c$ *scaling decoupled from the electronic coherence in iron-based superconductors,* Phys. Rev. B **98**, 020502 (2018).

[19] C. C. Homes, Y. M. Dai, J. S. Wen, Z. J. Xu, and G. D. Gu, $\mathrm{fete}_{0.55}\mathrm{se}_{0.45}$*: A multiband superconductor in the clean and dirty limit,* Phys. Rev. B **91**, 144503 (2015).

[20] M. Bendele, S. Weyeneth, R. Puzniak, A. Maisuradze, E. Pomjakushina, K. Conder, V. Pomjakushin, H. Luetkens, S. Katrych, A. Wisniewski, R. Khasanov, and H. Keller, *Anisotropic superconducting properties of single-crystalline* $fese_{0.5}te_{0.5}$, Phys. Rev. B **81**, 224520 (2010).

[21] B. Jäck, M. Eltschka, M. Assig, A. Hardock, M. Etzkorn, and C. R. Ast, *A nanoscale gigahertz source realized with Josephson scanning tunneling microscopy,* App. Phys. Lett. **106**, 013109 (2015).

[22] Y. Ota, N. Nakai, H. Nakamura, M. Machida, D. Inotani, Y. Ohashi, T. Koyama, and H. Matsumoto, *Ambegaokar-baratoff relations for josephson critical current in heterojunctions with multigap superconductors,* Phys. Rev. B **81**, 214511 (2010).

[23] Z. K. Liu, M. Yi, Y. Zhang, J. Hu, R. Yu, J.-X. Zhu, R.-H. He, Y. L. Chen, M. Hashimoto, R. G. Moore, S.-K. Mo, Z. Hussain, Q. Si, Z. Q. Mao, D. H. Lu, and Z.-X. Shen, *Experimental observation of incoherent-coherent crossover and orbital-dependent band renormalization in iron chalcogenide superconductors,* Phys. Rev. B **92**, 235138 (2015).

[24] U. R. Singh, S. C. White, S. Schmaus, V. Tsurkan, A. Loidl, J. Deisenhofer, and P. Wahl, *Spatial inhomogeneity of the superconducting gap and order parameter in* $fese_{0.4}te_{0.6}$, Phys. Rev. B **88**, 155124 (2013).

[25] D. L. Feng, D. H. Lu, K. M. Shen, C. Kim, H. Eisaki, A. Damascelli, R. Yoshizaki, J.-i. Shimoyama, K. Kishio, G. D. Gu, S. Oh, A. Andrus, J. O'Donnel, J. N. Eckstein, and Z.-X. Shen, *Signature of superfluid density in the single-particle excitation spectrum of bi2sr2cacu2o8+* δ, Science **289**, 277 (2000).

[26] Y. Kohsaka, C. Taylor, P. Wahl, A. Schmidt, J. Lee, K. Fujita, J. W. Alldredge, K. McElroy, J. Lee, H. Eisaki, S. Uchida, D.-H. Lee, and J. C. Davis, *How cooper pairs vanish approaching the mott insulator in bi 2 sr 2 cacu 2 o 8+ δ*, Nature **454**, 1072 (2008).

[27] W. Ruan, X. Li, C. Hu, Z. Hao, H. Li, P. Cai, X. Zhou, D.-H. Lee, and Y. Wang, *Visualization of the periodic modulation of cooper pairing in a cuprate superconductor,* Nature Physics **14**, 1178 (2018).

[28] Y. Dubi, Y. Meir, and Y. Avishai, *Nature of the superconductor–insulator transition in disordered superconductors,* Nature **449**, 876 (2007).

[29] I. Bloch, J. Dalibard, and W. Zwerger, *Many-body physics with ultracold gases,* Rev. Mod. Phys. **80**, 885 (2008).

[30] M. Randeria and E. Taylor, *Crossover from bardeen-cooper-schrieffer to bose-einstein condensation and the unitary fermi gas,* Annu. Rev. Condens. Matter Phys. **5**, 209 (2014).

[31] B. Sacépé, T. Dubouchet, C. Chapelier, M. Sanquer, M. Ovadia, D. Shahar, M. Feigel'man, and L. Ioffe, *Localization of preformed cooper pairs in disordered superconductors,* Nature Physics **7**, 239 (2011).

[32] Y. Cao, V. Fatemi, S. Fang, K. Watanabe, T. Taniguchi, E. Kaxiras, and P. Jarillo-Herrero, *Unconventional superconductivity in magic-angle graphene superlattices,* Nature **556**, 43 (2018).

[33] N. Reyren, S. Thiel, A. D. Caviglia, L. F. Kourkoutis, G. Hammerl, C. Richter, C. W. Schneider, T. Kopp, A.-S. Rüetschi, D. Jaccard, M. Gabay, D. A. Muller, J.-M. Triscone, and J. Mannhart, *Superconducting Interfaces Between Insulating Oxides,* Science **317**, 1196 (2007).

[34] J. Šmakov, I. Martin, and A. V. Balatsky, *Josephson scanning tunneling microscopy,* Phys. Rev. B **64**, 212506 (2001).

[35] B. D. Josephson, *Possible new effects in superconductive tunnelling,* Physics Letters **1**, 251 (1963).

[36] M. Tinkham, *Introduction to superconductivity* (McGraw-Hill, Inc. New York, 1996).

[37] V. Ambegaokar and A. Baratoff, *Tunneling between Superconductors,* Phys. Rev. Lett. **10**, 486 (1963).

[38] C. C. Tsuei and J. R. Kirtley, *Pairing symmetry in cuprate superconductors,* Rev. Mod. Phys. **72**, 969 (2000).

[39] T. K. Ng and N. Nagaosa, *Broken time-reversal symmetry in josephson junction involving two-band superconductors,* EPL (Europhysics Letters) **87**, 17003 (2009).

[40] Y. Ota, M. Machida, T. Koyama, and H. Matsumoto, *Theory of heterotic superconductor-insulator-superconductor josephson junctions between single- and multiple-gap superconductors,* Phys. Rev. Lett. **102**, 237003 (2009).

[41] P. Seidel, *Josephson effects in iron based superconductors,* Superconductor Science and Technology **24**, 043001 (2011).

[42] S.-Z. Lin, *Josephson effect between a two-band superconductor with $s++$ or $s\pm$ pairing symmetry and a conventional s-wave superconductor,* Phys. Rev. B **86**, 014510 (2012).

[43] O. Naaman, R. C. Dynes, and E. Bucher, *Josephson effect in pb/i/nbse 2 scanning tunneling microscope junctions,* International Journal of Modern Physics B **17**, 3569 (2003).

[44] P. W. Anderson, *Lectures on the Many-body Problem* (Academic Press, New York, 1964).